

1
2
3
4
5
6
7
8
9
10
11
12
13
14
15
16
17
18
19
20
21
22
23
24
25
26
27
28
29
30
31
32
33
34
35
36
37

Yttria-Stabilized Zirconia Aided Electrochemical Investigation on Ferric Ions in Mixed Molten Calcium and Sodium Chlorides

HONGBO HU,^{1,2} YUNMING GAO,^{1,2,*} YIGUI LAO,^{1,2} QINGWEI QIN,^{1,2}
GUANGQIANG LI,^{1,2} and GEORGE Z. CHEN^{1,2,3}

1. The State Key Laboratory of Refractories and Metallurgy, Wuhan University of Science and Technology, Wuhan 430081, China.
2. Key Laboratory for Ferrous Metallurgy and Resources Utilization of Ministry of Education, Wuhan University of Science and Technology, Wuhan 430081, China.
3. Department of Chemical and Environmental Engineering, and Energy Engineering Research Group, Faculty of Science Engineering, University of Nottingham Ningbo China, Ningbo 315100, China.

*Corresponding Author E-mail: gaoyunming@wust.edu.cn

38
39
40
41
42
43
44
45
46
47
48
49
50
51
52
53
54
55
56
57
58
59
60
61
62
63
64
65
66
67
68
69
70
71
72
73
74

ABSTRACT

Electrolytic reduction of dissolved iron oxide to metal iron in molten salts with an inert anode is an alternative short route for steelmaking without CO₂ emissions. A novel and simple integrated yttria-stabilized zirconia (YSZ) cell was constructed from a YSZ tube with a closed end. The YSZ tube played multiple functions, including the container for the molten salts, the solid electrolyte membrane in the O²⁻ | YSZ | Pt | O₂ (air) reference electrode (RE), and the solid electrolyte membrane between the working and counter electrodes (WE and CE). Electrochemical behavior of ferric ions (Fe³⁺) that were formed by dissolution of 0.5 wt pct Fe₂O₃ in the molten CaCl₂-NaCl eutectic mixture was investigated on a Pt WE at 1273 K by various electrochemical techniques including cyclic voltammetry, linear scan voltammetry, square wave voltammetry, chronopotentiometry, chronoamperometry, and potentiostatic electrolysis. Analysis of the mechanism of electrode reactions was further assisted by scanning electron microscopy, energy dispersive X-ray spectroscopy, and X-ray diffraction. Some electrochemical parameters were obtained, including the number of exchanged electrons and the diffusion coefficient of ferric ions in the mixed molten salts. The results from various electrochemical techniques are in good agreement with each other, and show that the electrochemical reduction of Fe³⁺ to Fe in the molten salt mixture could be a single three-electron transfer step and diffusion controlled reaction that was also possibly reversible. This work may form the foundation for extraction of iron and alloys from molten salts and also provide a stable O²⁻ | YSZ | Pt | O₂ (air) RE with wide applicability for investigation on electrochemical properties of other electroactive metal oxides in molten salts.

KEY WORDS: electrochemical behavior; ferric ions; molten salt; electrodeposition; reference electrode; zirconia-based solid electrolyte

75 I. INTRODUCTION

76 The current industrial approach to iron and steel smelting is a multi-step, long and complex,
77 and energy and emission intensive process. Firstly, the molten iron is produced from carbothermic
78 reduction of iron ore in the blast furnace (ca. 1773 K), and then steel is derived from
79 decarburization of the molten iron in the basic oxygen furnace (ca. 1873 K), followed by refining
80 and alloying. Electrolytic reduction of iron compounds (mainly halides or oxides) in molten salt
81 electrolyte using an inert oxygen-evolving anode is an alternative and short process for
82 ironmaking without CO₂ emissions.^[1-9] Aiming to drastically reduce CO₂ emissions, Europe has
83 set up an ultra-low CO₂ steelmaking (ULCOS) program which includes electrolytic reduction in
84 molten salts.^[10,11] Molten oxide electrolysis (MOE, ca. 1873 K) was proposed for production of
85 liquid iron in the United States.^[12-16] Also, direct electrolytic reduction of solid iron oxide bulk in
86 molten salts, *i.e.*, the Fray-Farthing-Chen (FFC) Cambridge process (ca. 1173 K), has also been
87 extensively investigated in laboratory.^[17-21] It is worth noting that molten salt electrolysis proceeds
88 at much lower temperatures and hence should incur less heat loss than the other processes.

89 Since iron can be extracted from molten salts at medium temperatures, and Fe₂O₃ is a
90 resourceful and low-cost raw material, electrolytic production of iron from Fe₂O₃ dissolved in
91 molten salts has drawn increasing attention in recent years. Electrochemical behavior of Fe³⁺ ions
92 in molten salts has been studied by some researchers and some findings have been obtained from
93 these early studies.^[6-9] However, it is difficult to draw an unambiguous conclusion from these
94 early studies because different experimental conditions were applied, including molten salt
95 composition, solute concentration, and temperature. In addition, the use of different working
96 electrodes (WEs) and reference electrodes (REs) in the early studies also made it inconvenient to
97 make systematic and comprehensive comparisons. Particularly, the reliability of potential values is
98 still in doubt when measured against those pseudo-REs of metal wires in molten salts.^[22,23]

99 Zirconia (ZrO₂) doped with magnesia (MgO), yttria (Y₂O₃), or the like is a kind of solid
100 electrolyte (shorted as MSZ or YSZ, *etc.*) that is featured by high conductivity to O²⁻ ions,
101 insignificant electronic conductivity, and good resistance to erosion by molten salts at high
102 temperatures. These zirconia-based solid electrolytes are widely used in the metallurgical industry
103 and fundamental research.^[24-39] For example, they are used to help the determination of the
104 activity^[24,25] and diffusion coefficient^[26,27] of oxygen in molten metals, and of the activity of FeO
105 in molten slags,^[28,29] to assist the electrolytic refining of molten metals,^[30,31] and the extraction of
106 metals from metal oxides dissolved in molten salts and slags.^[32-36] Furthermore, in order to
107 conduct electrochemical research on molten media containing O²⁻ ions, MSZ or YSZ can also be
108 used to construct a stable RE, such as the “O²⁻ | MSZ (or YSZ) | Pt | O₂ (air)” RE at high
109 temperatures.^[37-39] Since the O₂ partial pressure is very stable in the air, either stationary or
110 flowing, the O²⁻ | MSZ (or YSZ) | Pt | O₂ (air) RE is preferred for its good stability and
111 reproducibility. However, this type of RE is seldom applied to the fundamental electrochemical
112 analysis of molten salts to date.^[40-42]

113 We recently utilized an MSZ tube to fabricate an integrated electrochemical cell with the O^{2-} |
114 MSZ | Pt | O_2 (air) RE similar to the one used by Pal *et al.*,^[38] which is simple and unique in
115 structure and fabrication. With multiple functions such as the container for molten slags, and the
116 electron insulating but ion conducting membrane to separate the anolyte and catholyte, the MSZ
117 tube with a closed end was successfully applied to the electrochemical analyses in molten slags
118 containing FeO or NiO at ultra-high temperatures.^[43,44]

119 It is known that the O^{2-} ion conductivity of YSZ is usually higher than that of MSZ at the same
120 temperature. Thus, it was thought that YSZ could offer a sufficiently high O^{2-} ion conductivity at
121 temperatures lower than what is needed for MSZ to achieve the same conductivity. In this work, a
122 YSZ tube with a closed end was used to build an integrated electrochemical cell with the “ O^{2-} |
123 YSZ | Pt | O_2 (air)” RE for a systematic investigation on the property of Fe^{3+} ions on a Pt WE in
124 the molten $CaCl_2$ -NaCl eutectic mixture^[45] containing dissolved 0.5 wt pct Fe_2O_3 at 1273 K. The
125 experimentally determined operating temperature range in this work was from 1173 K to 1373 K
126 to enable sufficient oxide ion conductivity of the YSZ tube, and also to avoid significant
127 evaporation of the molten salt and attack to the YSZ tube by the molten salt.

128 Various electrochemical techniques were applied, such as cyclic voltammetry/voltammogram
129 (CV), linear scan voltammetry/voltammogram (LSV), square wave voltammetry/voltammogram
130 (SWV), chronopotentiometry/chronopotentiogram (CP), chronoamperometry/chronoamperogram
131 (CA), and potentiostatic electrolysis. Here, the $CaCl_2$ -NaCl eutectic mixture was chosen as the
132 medium in terms of source, cost, and wide application. Chen^[46] and Haarberg *et al.*^[47] studied the
133 solubility of Fe_2O_3 in $CaCl_2$ -NaCl melt, respectively. It can be reasonably assumed from their
134 work that the solubility of Fe_2O_3 in the molten $CaCl_2$ -NaCl eutectic mixture is above 1.5 wt pct at
135 1273 K and the Fe ions mainly exist in the +3 valence in the present work.

136 This work is part of an ongoing systematic research program aiming at developing a green
137 electrolytic process for iron- and steelmaking without emission of CO_2 . In the research, a YSZ
138 tube with a closed end was employed as the container of the molten salts, and also as the ion
139 conducting but electron insulating membrane to electronically and physically separate the WE and
140 CE. The YSZ tube was attached with a Pt CE and an “ O^{2-} | YSZ | Pt | O_2 (air)” RE (in fact an
141 “ O^{2-} | O_2 ” RE) on the external wall, forming a simple integrated electrochemical cell. In the work of
142 Pal *et al.*,^[32-34] the solid oxide membrane (SOM) was a tube with a closed end which was
143 immersed in the molten salt and acted only as the ion conducting to electronically and physically
144 separate the anode and cathode. Specifically, their SOM was not used to incorporate the RE.
145 Consequently, the SOM cell of Pal *et al.* was mainly used for electrolysis for metal extraction,
146 while the integrated cell is designed to enable various electrochemical analyses in high-
147 temperature melts.

148 The goal of the current investigation is to demonstrate the use of the novel integrated cell as a
149 simple and convenient tool for studying the electrochemical behavior of iron oxide dissolved in
150 molten salts, while we hope that the findings reported in the work will benefit similar studies of

151 other high-temperature electrolytes and the future design of the industrial cell capable of
152 continuous operation, and the selection, monitor, and control of the process variables for optimal
153 production.

154

155 II. EXPERIMENTAL

156 A. Preparation of Salt Specimen

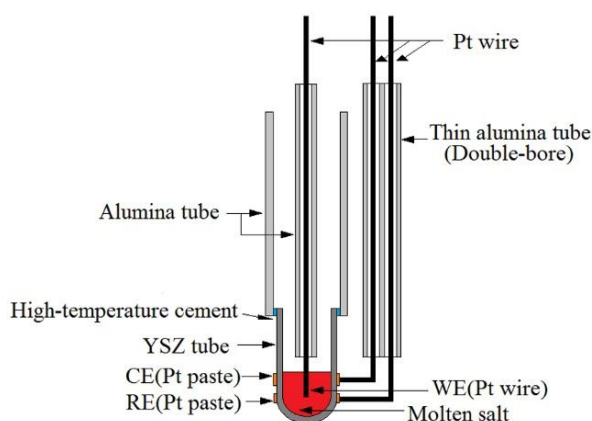
157 All chemical reagents used in this work were granules or powders of the analytical grade. In
158 order to avoid proportioning deviation caused by moisture absorption, a dehydration test was first
159 conducted at a chamber-type resistance furnace, in which the as-received powders of CaCl_2 and
160 NaCl were heated to and held at 773 K for 5 hours and the moisture contents were estimated to be
161 3.4 and 1.05 wt pct, respectively, according to weight loss of the heated salts. When weighing a
162 salt mixture with 65 wt pct CaCl_2 and 35 wt pct NaCl ,^[45] the moisture content was subtracted from
163 the raw reagents. The Fe_2O_3 reagent was heated at 473 K for 2 hours in a vacuum-drying-oven
164 with absolute pressure below 133 Pa. The dried Fe_2O_3 was added to the salt mixture of
165 CaCl_2 - NaCl to reach the composition of 0.5 wt pct Fe_2O_3 . The mixed salts and oxide powders
166 were subjected to ball milling in a sealed polyurethane jar with agate balls on a horizontal roller
167 for 3 hours at 25 RPM to ensure uniform mixing. After milling and separation from the agate balls
168 on a clean 8-mesh SS screener, the CaCl_2 - NaCl - Fe_2O_3 mixture was ready for use, or stored in a
169 desiccator for future purposes.

170

171 B. Construction of Electrochemical Cell

172 The integrated electrochemical cell was made from a YSZ (Y_2O_3 , 8 mol pct) tube with one
173 closed end and three electrodes, as schematically illustrated in Figure 1.

174



175

176 Fig. 1—Schematic illustration of the YSZ-based integrated three-electrode cell for
177 electrochemical analyses in molten salts at high temperatures (1273 K in this work).

178

179 The YSZ tube was supplied by Tianchang Hainas instrument Co., Ltd., where the YSZ tube

180 was prepared by isostatic pressing finely synthetic YSZ powder and sintering, and where the
181 synthetic YSZ powder was also purchased from outside. The size of YSZ tube used was 6.7 and
182 9.6 mm in inner and outer diameter, respectively, and 100 mm in length. The Pt paste (supplied by
183 Sino-Platinum Metals Co., Ltd, China) was uniformly painted on two adjacent circular parts of the
184 outer surface of the YSZ tube near the closed end. The Pt paste-painted YSZ tube was then dried
185 in the air, followed by sintering in air for 30 minutes in the chamber-type resistance furnace at
186 1173 K. Thus, two circular electrodes with good adhesion to the YSZ tube could be obtained. The
187 circular Pt electrode near the bottom was the RE (area: 0.91 cm²), and the other was the CE (area:
188 1.52 cm²). A long Pt wire (purity: 99.95 pct; diameter: 0.5 mm) lead was fastened to the YSZ tube
189 with a thin Pt wire (diameter: 0.3 mm) at each of the two circular Pt electrodes. The Pt wire leads
190 for the RE and CE and a Pt wire WE (diameter: 0.5 mm) were each protected in a thin alumina
191 tube.

192

193 *C. Experimental Methods*

194 Experimental data were measured and recorded on an electrochemical workstation (model:
195 IviumStat.h, Holland). The integrated electrochemical cell loaded with 1.25 g mixed salt was
196 placed in the thermostatic zone of a SiC high-temperature tube furnace (alumina furnace tube
197 inner diameter: 40 mm). High-purity argon (99.999 pct) was introduced through the silica-gel
198 desiccant for drying at flow rates of 300 and 10 mL min⁻¹ into the furnace tube from the bottom,
199 and into the YSZ tube from the top, respectively. A Pt-Rh (10 wt pct) | Pt thermocouple (Type S)
200 was employed to detect the experimental temperature. The furnace heating was programmed to
201 rise at a rate of 9 K min⁻¹. During heating, the heating program was held at 673 K and 873 K for 1
202 hour, respectively, to remove the moisture in the salt mixture, and also at 1273 K for 2 hours to
203 allow complete melting of the CaCl₂-NaCl-Fe₂O₃ mixture. Then, the Pt wire WE was inserted into
204 the melt, and the liquid level of the melt was determined by monitoring the open-circuit potential
205 (OCP) which became stable once the Pt wire touched the surface of the melt. The depth of the Pt
206 wire was controlled in the melt to 7 mm (contact area: 0.11 cm²). The Ar gas in the furnace tube
207 was subsequently switched to the high-purity synthetic air (containing 20.8 pct O₂ and 79.2 pct
208 N₂) at the rate of 300 mL min⁻¹. This was to maintain a stable O₂ partial pressure outside the YSZ
209 tube that is needed for the “O²⁻ | YSZ | Pt | O₂ (air)” RE to work.

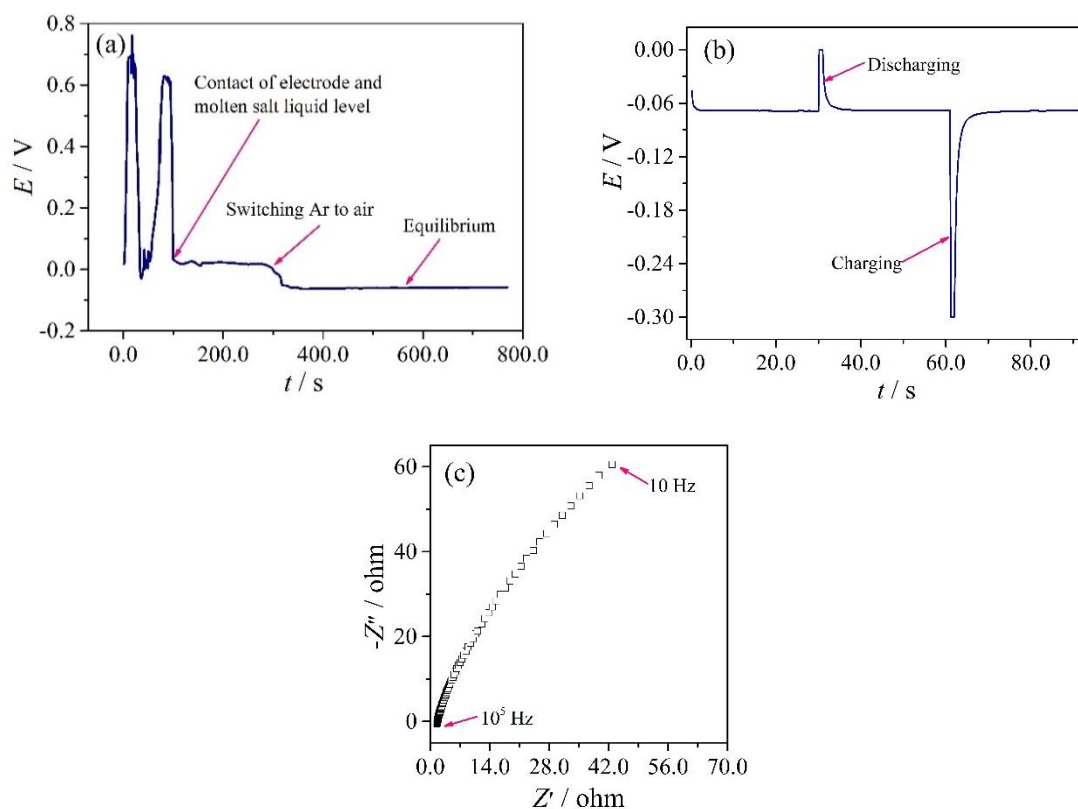
210 Figure 2(a) presents a typical OCP-time plot recorded in the course of immersing the Pt wire
211 WE into the melt and then switching from Ar to dry air in the furnace chamber. It can be observed
212 that, when the WE contacted the liquid level, the OCP instantaneously became stable. When the
213 atmosphere in the furnace tube was switched, the OCP slowly fell (the falling speed was related to
214 inner diameter of the furnace tube and the air flow rate), and finally stabilized at about -90 mV.
215 This result indicates that the “O²⁻ | YSZ | Pt | O₂ (air)” RE could work well and respond quickly to
216 the change of oxygen partial pressure in the furnace tube.

217 In order to test the reversibility of the RE in this work, a polarization experiment was also

218 carried out. The cell was discharged by short-circuiting, and then charged by an external current
 219 for 1 second, respectively. The WE potential responded quickly as shown in Figure 2(b). However,
 220 when the short-circuiting or the external current was removed, the WE potential returned to the
 221 initial OCP value within 3 seconds, as shown in Figure 2(b). The polarization result indicates that
 222 the “O²⁻ | YSZ | Pt | O₂ (air)” RE had a good reversibility.

223 After the OCP-time curve became stable, the total resistance of the melt and the YSZ
 224 membrane between the WE and RE was first measured by the alternating current (AC) impedance
 225 method (range and number of frequencies: 10⁵~10 Hz and 121, amplitude: 0.025 V, the OCP was
 226 taken as the applied bias potential). Figure 2(c) is a typical AC impedance Nyquist plot, showing a
 227 resistance of 1.64 ohm at the high frequency end, which was taken as the resistance value for the
 228 positive feedback compensation in all relevant electrochemical analyses.

229



230

231

232 Fig. 2—A typical OCP-time plot recorded in the course of immersing the Pt wire WE into the
 233 molten mixture containing 0.5 wt pct Fe₂O₃ and then switching from Ar to air in the furnace tube
 234 (a); a typical WE potential-time curve recorded in the polarization experiment (b), and a typical
 235 AC impedance Nyquist plot recorded at the OCP (bias potential) (c). RE: O²⁻ | YSZ | Pt | O₂ (air).

236

237 In the experiment, the OCP-time curve was always measured to determine if the cell had
 238 reached at a relatively stable state (usually, the OCP could fluctuate within 10 mV). Also, if
 239 necessary, the AC impedance measurement was repeated. It was found that the resistance from
 240 repeated measurements was fairly stable in the range of 1.64±0.08 ohm. Following these analyses,

241 a CV was usually recorded first, and repeated when needed, to confirm if the cell was in a stable
242 state. Other electrochemical measurements were then conducted sequentially. No visually
243 noticeable change for the YSZ tube used was observed after experiments. All potentials in this
244 work were reported with reference to the “O²⁻ | YSZ | Pt | O₂ (air)” RE.

245 In order to examine the structural features and the morphology of the reduction products, two
246 potentiostatic electrolysis experiments were carried out, in which a Pt wire and a Pt foil (30 mm ×
247 2 mm × 0.1 mm) were employed as the WE, respectively. Each electrolysis experiment was
248 carried out for 30 minutes at the reduction potential of about -0.7 V based on the CV. When using
249 the Pt foil WE, the amount of the melt in the YSZ tube increased to 2.00 g, the area of CE on the
250 outer surface of the YSZ increased to 4.56 cm², and the depth of the Pt foil in the melt was
251 controlled to be 15 mm. Other conditions were the same as the experiments for electrochemical
252 analyses as mentioned above.

253 After potentiostatic electrolysis, the Pt WE was separated from the solidified melt, and
254 repeatedly washed, under sonication, in distilled water and absolute ethyl alcohol in succession to
255 remove residual salts attached to the surface of the WE. A short piece was cut from the portion of
256 the Pt wire WE immersed in the melt. It was then mounted in epoxy resin to enable examination
257 of the cross section of the electrode by scanning electron microscopy (SEM) (Nova 400 Nano)
258 equipped with energy dispersive spectrometry (EDS) (INCAIE 350 Penta FET X-3). For the Pt
259 foil WE, the surface phase was analyzed by X-ray diffraction (XRD, Cu K α , Philips Xpert Pro
260 MPD). Due to the requirement of XRD analyses for sample size, the Pt foil was cut and re-joined
261 to increase the width from 2 to 4 mm and decrease the length from 15 mm (original depth in the
262 melt) to about 8 mm.

263

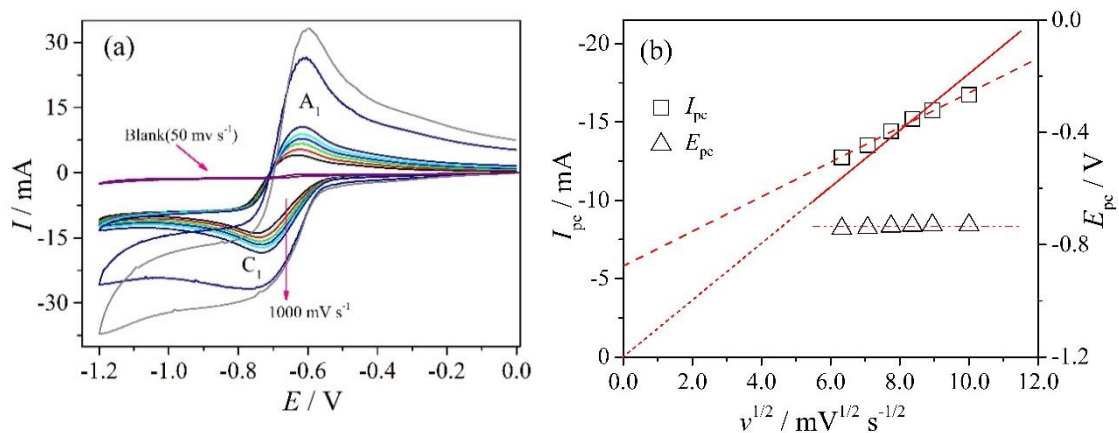
264 **III. RESULTS AND DISCUSSION**

265 *A. Cyclic Voltammetry*

266 Figure 3(a) presents the CVs recorded in the molten CaCl₂-NaCl eutectic mixture with 0.5 wt
267 pct Fe₂O₃ recorded at an increasing potential scan rate, ν , and that recorded without Fe₂O₃ (*i.e.*, the
268 blank melt) at 50 mV s⁻¹ and 1273 K. It is observed on the CV that, within the potential range
269 scanned, the current of the blank melt is basically zero, indicating negligible redox active
270 impurities and good electrochemical stability of both the blank melt and the WE in this potential
271 range. In presence of Fe₂O₃, the current on the CV smoothly increases at first with negative
272 potential scan, and then rapidly increases to form a reduction peak C₁. After reversing the scan, an
273 oxidation peak A₁ appears.

274 Because C₁ and A₁ are both absent on the CV in the blank melt, they must have been related
275 with dissolved Fe₂O₃ and may be attributed to the reduction of the Fe³⁺ ion and the re-oxidation of
276 the reduction product, *e.g.* Fe. The concentration of Fe₂O₃ in the molten CaCl₂-NaCl mixture was
277 0.5 wt pct which is equivalent to a mole fraction of 2.5×10⁻³. For approximation, this mole fraction

278 was assumed to be the activity of Fe_2O_3 in the melt, while the activity of Fe on the electrode was
 279 assumed to be unity. Thus, calculation of the decomposition voltage could be conducted under an
 280 O_2 partial pressure of 20.8 kPa for the RE using the thermodynamic software Factsage.^[48] Under
 281 the applied conditions, the calculated decomposition voltage of $\text{Fe}_2\text{O}_3 \rightarrow 2\text{Fe} + 1.5\text{O}_2$ is -0.791 V
 282 which is lower than that of any other component in the melt. In fact, only the oxide can be reduced
 283 under the condition of the ion conducting membrane. Because all electrochemical analyses were
 284 carried out against the $\text{O}^{2-} | \text{YSZ} | \text{Pt} | \text{O}_2$ (air) RE, it is reasonable to take the decomposition
 285 voltage of -0.791 V for Fe_2O_3 as the reduction potential of Fe^{3+} to Fe. For the CVs, with some
 286 basic assumptions, it can be calculated that the formal potential is -0.680 V.
 287



288
 289 Fig. 3—CVs recorded in molten $\text{CaCl}_2\text{-NaCl}$ at 1273 K with 0.5 wt pct Fe_2O_3 at v (potential scan
 290 rate) = 0.04, 0.05, 0.06, 0.07, 0.08, 0.10, 0.50, or 1.00 V s^{-1} , and without Fe_2O_3 (blank) at $v = 50$
 291 mV s^{-1} (a), and correlations of I_{pc} (reduction peak current) and E_{pc} (reduction peak potential) with
 292 $v^{1/2}$ (b). RE: $\text{O}^{2-} | \text{YSZ} | \text{Pt} | \text{O}_2$ (air).
 293

294 Since only one pair of oxidation-reduction peaks, A_1 and C_1 , can be seen on the CVs in Figure
 295 3(a), and the half-peak potential of peak C_1 is -0.649 V (at 40 mV s^{-1}) which is sufficiently close to
 296 the calculated formal potential of -0.680 V, it is reasonable to attribute peak C_1 to the one-step
 297 reduction of $\text{Fe}^{3+} + 3e \rightarrow \text{Fe}$. There may be two reasons for observed and calculated potentials for
 298 peak C_1 . Firstly, the actual activity of Fe_2O_3 in the melt could be larger than the mole fraction.
 299 Secondly, the deposited Fe could alloy with the Pt electrode as indicated by the Fe-Pt phase
 300 diagram,^[49] resulting in a Fe activity lower than unity during the initial reduction.

301 As shown in Figure 3(a), electroactive species in the melt can be reduced or oxidized and the
 302 corresponding redox peaks arise in the case of scanning the potential. The current of the cell, that
 303 is, the oxygen-ion current passing through the YSZ membrane, does not increase/decrease at all
 304 times with applied potential. Rather, it changes with the reactions of the electroactive species.
 305 Obviously, the transport, including electromigration, of O^{2-} ions in the YSZ membrane does not

306 affect the behavior of electroactive species on the Pt WE in the three-electrode cell at
307 sufficiently high temperature. However, in a future industrial two-electrode cell, the transports of
308 oxygen ions through the YSZ membrane may be highly likely an important factor affecting the
309 rate of the overall process. It is worth noting that the shapes of peaks C₁ and A₁ on the CVs
310 indicate that the reduction products could be soluble,^[50] and the physical state of the reduction
311 products will be analyzed later by means of correlation detection.

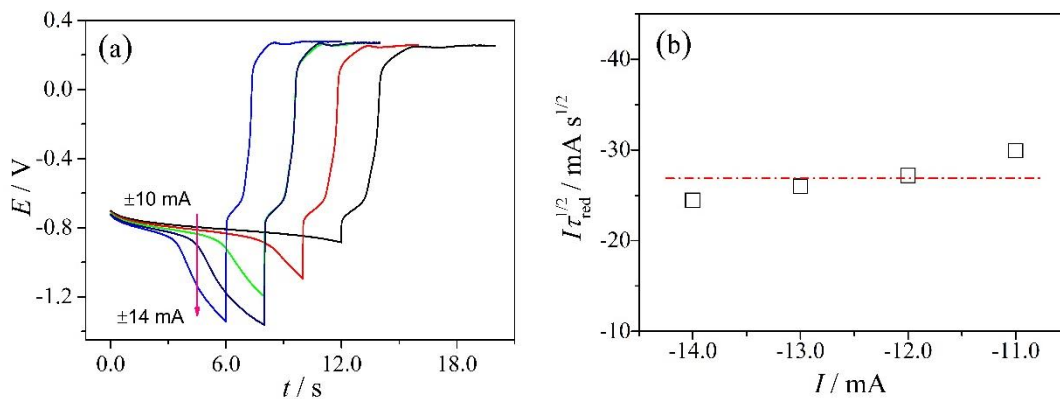
312 In order to evaluate the reversibility of electrode process, the CV tests were performed at
313 different scan rates. Figure 3(a) shows that with the potential scan rate increasing from 0.04 to 0.1
314 V s⁻¹. The ratio of the oxidation and reduction peak currents (base current subtracted), I_{pa}/I_{pc} , is
315 close to unity, the reduction peak potential, E_{pc} , remains constant (~ -0.735 V) with increasing ν ,
316 while plotting I_{pc} vs $\nu^{1/2}$ produces a straight line whether or not the origin is passed, as shown in
317 Figure 3(b). These three observations indicate that the reduction of Fe³⁺ to Fe is diffusion
318 controlled and reversible.^[6,50,51] However, when ν increases from 0.1 to 0.5 ~ 1.0 V s⁻¹, E_{pc} shifts
319 negatively, and I_{pc} deviates noticeably from the $I_{pc} - \nu^{1/2}$ fitting straight line (the data from high
320 scan rates are not included in Figure 3(b), and I_{pa}/I_{pc} increases beyond 1. These CVs which result
321 from the reduction reaction of Fe³⁺ to Fe on the Pt electrode show the reversible shape at low scan
322 rates but the CV shape become less reversible or irreversible with increasing the scan rate.^[52] A
323 supplementary discussion on the reversibility of the reduction process is added in Section III-E.

324 To sum up, the reduction of Fe³⁺ to Fe on the Pt WE as represented by the CVs recorded at
325 relatively low potential scan rates is a one-step and diffusion-controlled reversible process. This
326 finding is consistent with the reported CVs of Fe³⁺ in molten CaCl₂-NaCl with molybdenum and
327 silver wires as the WE and RE, respectively, although the I_{pa}/I_{pc} ratio on the reported CVs was not
328 unity.^[6] It is acknowledged that it is yet uncertain whether the reduction-produced Fe was
329 dissolved in the melt or alloyed with the Pt WE. It is also necessary to check if there was any
330 reduction product and its physical state on the Pt WE before the CVs could be evaluated properly.
331 Hence, three measures were taken as described below.

332 Firstly, reversal CP was applied to investigate the redox couple of Fe³⁺/Fe in the melt and the
333 findings are shown in Figure 4(a). It can be seen that upon application of the constant negative
334 current, the potential fell initially and soon arrived at a plateau. The plateau potential, ca. -0.8 V, is
335 consistent with the potential of the Fe³⁺ reduction peak shown in Figure 3(a).

336 The shape of the reversal CP can be explained as follows. With the Fe³⁺ concentration
337 decreasing in the melt, the diffusion of Fe³⁺ to the electrode surface becomes slower than the
338 depletion of Fe³⁺ on the electrode surface. When the Fe³⁺ concentration on the electrode surface
339 falls to zero, the electrode potential changes quickly to more negative value where the next
340 reduction reaction occurs. Then, when an equal reverse current I is applied, the potential also
341 reverses quickly till another plateau where the previous reduction products are re-oxidized to Fe³⁺.
342 The difference between the applied currents is very small, and the amount of reduction products is
343 also very small. Also, the reduction-produced Fe dissolves into the Pt electrode to form a solid

344 solution (for details, see the follow – up). Thus, there is little difference in the activity of Fe on the
 345 surface of the solid solution, leading to very comparable overpotentials of the re-oxidation, as
 346 shown in Figure 4(a). The tilt of the re-oxidation plateau indicates that the activity of iron in the
 347 alloy decreases continuously during oxidation, which could be due to the fact that the Fe diffused
 348 into the Pt electrode was not oxidizable on the time scale of the CV. Upon completion of the
 349 re-oxidation of the reduction produced Fe on the electrode surface, the potential quickly changes
 350 to more positive values of about +0.2 V. It is supposed to be the oxidation of oxygen ions to
 351 oxygen molecule at potentials of about +0.2 V, where some fluctuations can be observed in Figure
 352 4(a), indicating the gas involved in the electrode reaction. This is related to the oxidation of the
 353 oxygen ion: $O^{2-} \rightarrow 1/2O_2 + 2e$. It should be noted that oxidation of oxygen ions in the melt was not
 354 further investigated in the positive potential range because the present work dealt mainly with the
 355 reduction of iron ions in the negative potential range.
 356

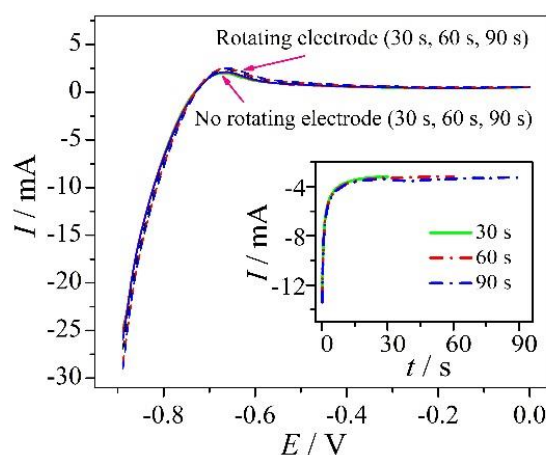


357
 358

359 Fig. 4—Reversal CPs on the Pt WE in molten $CaCl_2$ - $NaCl$ with 0.5 wt pct Fe_2O_3 at 1273 K and
 360 different currents (± 10 , ± 11 , ± 12 , ± 13 and ± 14 mA) (a) and the correlation of the $I\tau^{1/2}$ (τ
 361 transition time) value against the cathodic current I for the reduction plateau (b). RE: O^{2-} | YSZ | Pt
 362 | O_2 (air).
 363

364 The transition time for reduction or oxidation (τ_{red} or τ_{ox}) is basically the duration of the
 365 potential plateau in Figure 4(a). The data listed in Table I were measured using methods in
 366 accordance with the literature.^[53-55] It can be seen from Table I that, at 1273 K, increasing the
 367 applied current led to a quicker depletion of electroactive ions on the electrode surface, resulting
 368 in decreased values of τ_{red} and τ_{ox} . Table I also shows that the τ_{red}/τ_{ox} ratio also decreased from 6
 369 to 2.9, suggesting that increasing the applied current has a greater impact on the decrease of τ_{red}
 370 than that of τ_{ox} . According to the literature,^[55] at $\tau_{red}/\tau_{ox} = 1$, the reduction products should be
 371 insoluble; when $\tau_{red}/\tau_{ox} = 3$, soluble reduction products, usually in the liquid electrolyte, would be
 372 expected. In this work, however, $\tau_{red}/\tau_{ox} = 6 \sim 2.9$ ($\tau_{red}/\tau_{ox} = 7$ was reported in the literature ^[55])
 373 which makes it uncertain if the reduction products were insoluble (e.g. Fe) or soluble (e.g. Fe^{2+}).

374 Secondly, some experiments were carried out. In these experiments, upon confirmation of the
 375 electrochemical cell having reached the equilibrium or steady state as indicated by the OCP,
 376 potentiostatic electrolysis was performed at -0.76 V for a predetermined time of 30 seconds. Then,
 377 the OCP was monitored for 60 seconds (halting time), while the Pt WE was in two working modes:
 378 the usual static mode and the manually rotating mode with 2 circles. Then, anodic LSV was
 379 performed from -0.9 to 0 V at $\nu = 50 \text{ mV s}^{-1}$. The same procedure was repeated for another two
 380 predetermined times (60 and 90 seconds) of electrolysis at -0.76 V. Thus, the experiments
 381 produced six LSVs, as shown in Figure 5. In inset of Figure 5, typical curves of the potentiostatic
 382 electrolysis using the Pt wire WE for 30, 60, and 90 seconds are presented. In order to eliminate
 383 the influence of the residual products from the reduction, before the next test, the potentiostatic
 384 electrolysis was performed at 0.05 V for 90 seconds to oxidize all the materials deposited on the
 385 electrode surface in the previous test, where preliminary experiments indicated that the electrode
 386 was not oxidized and no new oxidation peak occurred. In addition, the preliminary experiments
 387 also indicated that the halting time from 15 to 360 seconds had no detectable effect on the LSVs
 388 recorded in the static mode.
 389



390
 391 Fig. 5—LSVs recorded at 50 mV s^{-1} on the Pt wire WE under the static and rotating modes after
 392 the potentiostatic electrolysis for 30, 60, 90 seconds in molten $\text{CaCl}_2\text{-NaCl}$ with 0.5 wt pct Fe_2O_3 .
 393 Inset: a set of typical current-time curves of potentiostatic electrolysis using the Pt wire WE for 30,
 394 60, 90 seconds. Potentiostatic electrolysis potential: -0.76 V; time: 30, 60, 90 s; temperature: 1273
 395 K; RE: O^{2-} | YSZ | Pt | O_2 (air).
 396

397 It is expected from these experiments that if the reduction products were soluble, they would
 398 not accumulate on the electrode surface and, consequently, no significant change on the anodic
 399 LSV would happen in the static mode even if the time of the potentiostatic reduction was doubled.
 400 Otherwise, if insoluble products were formed, doubling the time of the potentiostatic reduction
 401 should lead to likely a double increase of the re-oxidation current. If the Pt WE was rotated
 402 manually when measuring the OCP for 60 seconds (halting time), for reduction products soluble in

403 the melt, the diffusion flux of the products from the electrode surface into the melt would decrease
 404 in the following anodic LSV. However, if the reduction product could remain on the Pt WE due to
 405 alloying with Pt, the diffusion flux of the products from the surface into interior of the Pt WE
 406 would not markedly change. The current on the following LSV should correspond to the change of
 407 the diffusion flux. Consequently, following the potentiostatic reduction and the 60-second OCP
 408 measurement with the rotating Pt WE, changes of the oxidation peak on the anodic LSV can be
 409 used to judge if the reduction products dissolved in the melt.

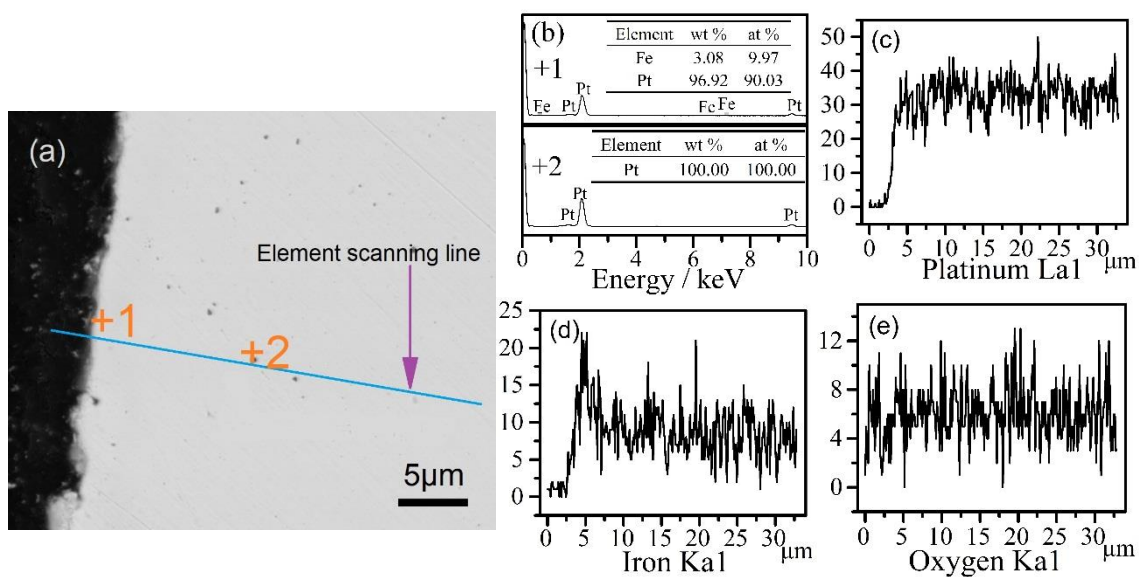
410 As can be observed in Figure 5, the anodic LSVs are highly consistent with each other under
 411 various conditions. Under the static mode, doubling the time of potentiostatic electrolysis did not
 412 lead to a higher current of the oxidation peak on the LSVs, suggesting that the reduction products
 413 could be soluble. However, it cannot be determined whether the reduction products dissolved in
 414 the melt or alloyed with the Pt electrode. Further, Figure 5 shows that the oxidation peak currents
 415 on the LSVs are also the same with or without rotating the Pt WE, indicating the reduction
 416 products having alloyed with Pt.

417 Thirdly, the Pt WE was characterized by SEM, EDS, and XRD after the potentiostatic
 418 electrolysis to identify the reduction products. Figure 6 shows the SEM image of the cross section
 419 of the Pt wire WE, the corresponding EDS, and the line scanning analyses of Pt, Fe, and O. As
 420 shown in Figure 6(b), the EDS analysis confirmed the presence of Fe on the Pt wire WE surface.
 421 Figure 6(d) presents the line scanning profile for Fe, confirming a maximum Fe content at the
 422 position of 0.5 μm from the Pt WE surface. Figure 7 shows the XRD pattern for the Pt foil WE
 423 after potentiostatic electrolysis. From Figure 7, the existence of the FePt_3 phase is not certain, but
 424 the independent pure Fe phase can be excluded. Therefore, based on the EDS analyses, it is
 425 believed that reduction-produced Fe could have reacted with the Pt electrode to form an alloy or
 426 intermetallic compound, *e.g.*, FePt_3 whose XRD pattern overlaps with that of Pt.

427

428

429



430

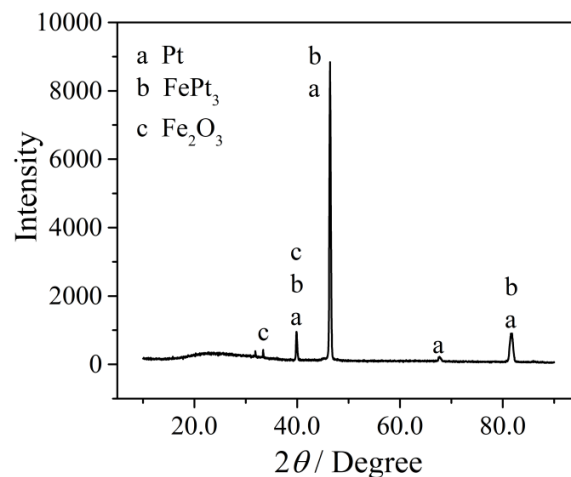
431

432 Fig. 6—SEM image of the cross section of the Pt wire WE (a), EDS analyses of spots 1 and 2 in
 433 the SEM image (b), and the line scanning profiles of Pt (c), Fe (d), and O (e) after potentiostatic
 434 electrolysis in molten CaCl₂-NaCl with 0.5 wt pct Fe₂O₃. Potentiostatic electrolysis potential: -
 435 0.73 V; time: 30 min; temperature: 1273 K; RE: O²⁻ | YSZ | Pt | O₂ (air).

436

437 The findings from SEM, EDS, and XRD are in agreement with that from the reversal CPs and
 438 the LSVs, confirming the reduction products to be Fe which, upon deposition, alloyed with the Pt
 439 WE. However, the fact that $I_{pa}/I_{pc} \approx 1$ as shown in Figure 3(a) suggests that the alloy formation
 440 had not caused a major impact on the derived parameters from the CVs.

441



442

443 Fig. 7—XRD pattern for the Pt foil WE after potentiostatic electrolysis in molten CaCl₂-NaCl
 444 with 0.5 wt pct Fe₂O₃. Potentiostatic electrolysis potential: - 0.7 V; time: 30 min; temperature:
 445 1273 K; RE: O²⁻ | YSZ | Pt | O₂ (air).

446

447 For a reversible electrode process with both soluble reactant and product, considering only
 448 semi-infinite linear diffusion, the number of exchanged electrons in the electrode reaction and the
 449 diffusion coefficient are usually calculated, respectively, from Eq. [1] and the Randles-Sevcik
 450 equation, that is, Eq. [2].^[56-60]

$$451 |E_p - E_{p/2}| = 2.2RT/(nF) \quad [1]$$

$$452 I_{pc} = -0.4463nFAC_0(RT)^{-1/2}(nFvD)^{1/2} \quad [2]$$

453 where E_p is the cathodic or anodic peak potential, V; $E_{p/2}$ the half-peak potential, V; n the number
 454 of exchanged electrons; F Faraday's constant, $F = 96500 \text{ C mol}^{-1}$; R the molar gas constant, $R =$
 455 $8.314 \text{ J mol}^{-1} \text{ K}^{-1}$; T the temperature, $T = 1273 \text{ K}$; A the area of WE, here $A = 0.11 \text{ cm}^2$; D the
 456 diffusion coefficient of electroactive species (Fe^{3+}), $\text{cm}^2 \text{ s}^{-1}$; I_{pc} the cathodic peak current, A; v the
 457 potential scan rate, V s^{-1} ; and C_0 is the molar concentration of electroactive species (Fe^{3+}), mol
 458 cm^{-3} . In this work, due to the very low Fe_2O_3 concentration ($C_0 = 1.10 \times 10^{-4} \text{ mol cm}^{-3}$), the density
 459 of the molten $\text{CaCl}_2\text{-NaCl}$ mixture with Fe_2O_3 at 1273 K can be expressed approximately by that

460 of the molten mixture alone (1.758 g cm^{-3}).^[61] It is assumed that the corrections related to
461 cylindrical geometry of the Pt wire WE can be neglected under the experimental conditions.

462 Specifically, in this work, the CVs showed three typical characteristics for reversible electrode
463 reactions justifying the use of Eqs. [1] and [2]. The EDS and XRD analyses show that the
464 reduction product does not exist in the form of an independent Fe phase, but rather forms an alloy
465 with the electrode. Here, the alloy formed between the precipitated Fe and the Pt electrode can be
466 regard as a solid solution. In other words, the reduction product is dissolved in the Pt electrode,
467 not an insoluble deposit. More importantly, the alloy formation was found to have no significant
468 effect on the above typical characteristics of reversible reaction. Therefore, Eqs. [1] and [2] were
469 applied to the reversible reaction with soluble reactant although the reduction product Fe was not
470 dissolved in the electrolyte but in the Pt electrode.

471 The numbers of exchanged electrons in the reaction of the cathodic and anodic peaks as
472 derived from Eq. [1] are $n_c = 2.6 \approx 3$ and $n_a = 2.8 \approx 3$, respectively. It can then ascertain that, on
473 the CVs, the cathodic peak corresponds to the one-step reduction of Fe^{3+} to Fe, and the anodic
474 peak to the re-oxidation of Fe to Fe^{3+} .

475 For a diffusion-controlled reversible reaction, it is well known that the relationship between
476 I_{pc} and $v^{1/2}$ accords with the Randles-Sevcik equation, that is, Eq. [2]. According to Eq. [2],
477 theoretically, the linear relationship between I_{pc} and $v^{1/2}$ should pass through the origin. However,
478 quite a few researchers found that was not the case, if only experimental data points were fitted in
479 a straight line. The discussion is as follows:

480 Firstly, there is some accompanying process (such as ion adsorption) in the electrode reaction,
481 which is parallel to the main Faraday process.^[2,62,63] In this case, the experimental data points,
482 excluding the origin, are fitted in a straight line and the intercept with a small positive value can
483 be obtained. These small positive values for intercepts cannot invalidate the deduction regarding
484 that the process is diffusion controlled. This fitting method is adopted by some researchers.^[2,62,63]

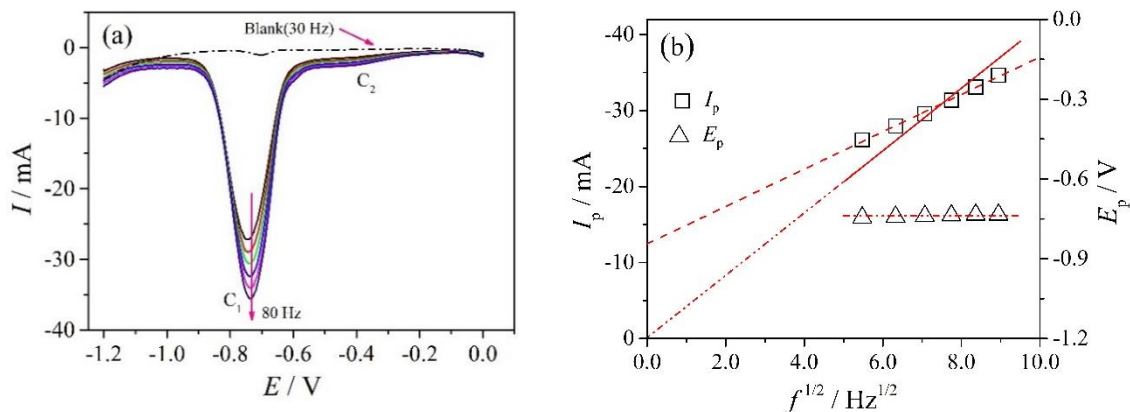
485 Secondly, there is a certain experimental error.^[64] In this case, according to Eq. [2],
486 theoretically, the linear relationship between I_{pc} and $v^{1/2}$ should pass through the origin. Therefore,
487 in order to reduce the error, the experimental data points, together with the origin point, are fitted
488 in a straight line within a desired accuracy. This fitting method is also adopted by some
489 researchers.^[53,54,64,65] It should be noted that the approach is theoretically in line with the
490 requirements of the Randles-Sevcik equation.

491 In this work, since both the parallel process of electrode reaction and experimental error are
492 considered to be uncertain, the experimental data points are fitted into a straight line with and
493 without passing through the origin for the convenience of comparison, as shown in Figure 3(b).
494 Thus based on Eq. [2], the diffusion coefficients can be derived from the slopes of linear fitting of
495 the $I_{pc} - v^{1/2}$ plot. They are found to be $(4.9 \pm 0.5) \times 10^{-5} \text{ cm}^2 \text{ s}^{-1}$ (passing through the origin) and
496 $(1.8 \pm 0.1) \times 10^{-5} \text{ cm}^2 \text{ s}^{-1}$ (not passing through the origin), respectively. The difference between the
497 two is not large and the two diffusion coefficient values are in the same order of magnitude.

498

499 B. Square Wave Voltammetry

500 Due to its high sensitivity, SWV is effective in suppressing the influence of the capacitive
501 background current as often observed on CV, particularly at relatively high scan rates. In this
502 experiment, in order to confirm the reversibility of electrode process and evaluate electrochemical
503 parameters such as the number of transferred electrons and diffusion coefficient, the SWV tests
504 were performed at different scan frequencies. The SWVs of the melt containing 0.5 wt pct Fe₂O₃
505 (including the blank melt) at 1273 K were measured at 1 mV in step potential and 30 mV in
506 amplitude, and different scan frequencies, as shown in Figure 8(a).



507

508

509 Fig. 8—SWVs recorded in the molten CaCl₂-NaCl mixture with 0.5 wt pct Fe₂O₃ at different
510 frequencies (30, 40, 50, 60, 70, 80 Hz) and 1273 K (a) and the correlations between the peak
511 current (I_p), the peak potential (E_p), and the square root of the frequency ($f^{1/2}$), respectively (b).
512 RE: O²⁻ | YSZ | Pt | O₂ (air).

513

514 Figure 8(a) shows that with negative scanning of the potential, the current starts to smoothly
515 increase, experiences a small peak C₂ first at -0.4 V, and then rapidly increases to the main
516 reduction peak C₁ at -0.74 V. The potential of C₁ is consistent with that of the reduction peak C₁
517 on the CVs in Figure 3(a), indicating its origin being the Fe³⁺ reduction. The peak C₂ in Figure 8(a)
518 is invisible on the blank SWV, and neither on the CVs in Figure 3(a), and hence the formation of
519 peak C₂ should have a relation with addition of Fe₂O₃. Frangini *et al.* [66] found that the addition of
520 0.5 mol pct La₂O₃ to the molten carbonate salt resulted in a dramatic increase of O₂ solubility.
521 Similarly, it is supposed that the addition of Fe₂O₃ could increase O₂ solubility in the melt in this
522 work. It is known that the dissolution of oxygen could lead to the formation of superoxide and
523 peroxide ions in molten salts at high temperatures and these ions could keep a dynamic
524 equilibrium of formation and dissociation.[66-69] Therefore, the peak C₂ might be ascribed to the
525 related reduction reaction of oxygen in the melt. Here the related reduction reaction of oxygen
526 means the reduction of intermediate oxide ion species such as superoxide and peroxide ions rather
527 than to simply molecular oxygen entities. However, the occurrence of the peak C₂ still needs to be
528 further explored.

529 With increasing the frequency f , the potential of Fe^{3+} reduction peak C_1 basically remains
 530 unchanged; by plotting and fitting the relation between the reduction peak C_1 current I_p (base
 531 current subtracted) and the square root of the frequency $f^{1/2}$ value, a linear correlation between I_p
 532 and $f^{1/2}$ is observed whether or not the origin is passed, as shown in Figure 8(b). It can
 533 comprehensively be judged that the reduction of Fe^{3+} corresponding to the peak C_1 is a reversible
 534 reaction in the melt with 0.5 wt pct Fe_2O_3 at 1273 K. Thus, within the range of the frequencies
 535 measured, the number of exchanged electrons and the diffusion coefficient of Fe^{3+} ions can be
 536 calculated from Eqs. [3] [53,54,58, 60,70,71] and [4], [72-76] respectively, as follows:

$$537 \quad W_{1/2} = 3.52RT/(nF) \quad [3]$$

$$538 \quad I_p = -0.31\pi^{-1/2}R^{-1}T^{-1}AC_0D^{1/2}n^2F^2\Delta Ef^{1/2} \quad [4]$$

539 where $W_{1/2}$ is the half-peak width, V, the peak is not exactly symmetric as predicted by theory, see
 540 the method from the literature [71] for taking $W_{1/2}$ value; f the frequency, Hz; and ΔE is the
 541 potential amplitude, V, here $\Delta E = 0.03$ V. Eqs. [3] and [4] are applicable to the reversible system
 542 with semi-infinite linear diffusion. It is known that Eq. [3] is valid if the peak current is linear with
 543 the square root of the frequency of the potential signal in SWV. [53,54,71] And Eq. [4] can be applied
 544 when the potential amplitude (ΔE) (30 mV in this work) in the SWV is smaller than the ratio of
 545 $RT/(nF)$. [74-77]

546 Based on Eq. [3], it can be derived from the fitting that the number of exchanged electrons n
 547 $= 2.7 \approx 3$, which suggests again this reduction peak C_1 corresponding to the reaction of one-step
 548 reduction of Fe^{3+} to Fe. In this work, similar to the above plot of I_{pc} against $v^{1/2}$ in the CVs (see
 549 Figure 3(b)), it can also be understood that a plot of I_p against $f^{1/2}$ yields a straight line with and
 550 without passing through the origin within a desired accuracy based on Eq. [4], as shown in Figure
 551 8(b). The diffusion coefficients derived from $I_p - f^{1/2}$ fitting straight line slope are $(6.7 \pm 0.4) \times 10^{-5}$
 552 $\text{cm}^2 \text{ s}^{-1}$ (passing through the origin) and $(2.4 \pm 0.1) \times 10^{-5} \text{ cm}^2 \text{ s}^{-1}$ (not passing through the origin),
 553 respectively. The two are also close and in the same order of magnitude.

554

555 C. Chronopotentiometry

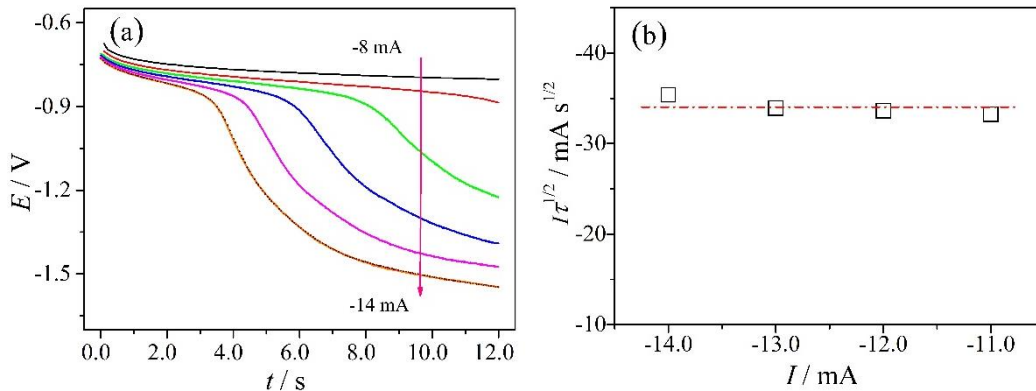
556 In order to determine whether the electrode process is controlled by diffusion, the CP tests
 557 were performed at different applied currents. Figure 9(a) shows the CPs recorded in the melt with
 558 0.5 wt pct Fe_2O_3 at 1273 K. It can be found that the characteristics on the CPs are exactly the same
 559 as that of reduction part on the reversal CPs (see Figure 4(a)) mentioned above. With increasing
 560 negative applied current, the depletion rate of Fe^{3+} on the surface of the electrode was quickened,
 561 and the reduction transition time τ also decreased slowly. Select easily readable data on reduction
 562 transition time, and draw the $I - I\tau^{1/2}$ plot, as shown in Figure 9(b).

563 From Figure 9(b), it can be observed that the measured $I\tau^{1/2}$ value varied insignificantly with
 564 the applied current I and matched closely to a horizontal straight line within a desired accuracy.
 565 Therefore, it can also be determined that the reduction of Fe^{3+} to Fe is a diffusion-controlled

566 process in the melt with 0.5 wt pct Fe₂O₃ at 1273 K. Based on the Sand Equation (Eq.
 567 [5]),^[53-55,59,60] the diffusion coefficient of Fe³⁺ is derived to be (7.5±0.6)×10⁻⁵ cm² s⁻¹.

$$568 \quad I\tau^{1/2} = -nFAC_0\pi^{1/2}D^{1/2}/2 \quad [5]$$

569 where I is the cathodic current (A); τ is the transition time (s). Eq. [5] is applicable to the case
 570 where the mass transport is controlled by semi-infinite linear diffusion at constant applied currents.
 571 It should be noted that the application of Eq. [5] is not dependent on the reversibility of reaction.
 572



573
 574 Fig. 9—CPs recorded in the melt with 0.5 wt pct Fe₂O₃ at 1273 K at different cathodic currents of
 575 -8, -10, -11, -12, -13, -14, -14 mA (a) and the correlation between the cathodic current I and the
 576 $I\tau^{1/2}$ (τ : transition time) value for the reduction plateau (b). RE: O²⁻ |YSZ | Pt | O₂ (air).

577
 578 In addition, it can be observed from Figure 9(a) that there is another reduction reaction at
 579 about -1.25 to -1.55 V. The attribution of the reduction reaction can be analyzed as follows:

580 In this work, since the YSZ membrane is used as the isolation membrane, only the iron ions
 581 from the added iron oxide can be electrolytically reduced in the melt; the chloride cannot be
 582 reduced. Besides Fe₂O₃ in the melt, there may also be a small amount of oxide impurities or newly
 583 formed oxides, such as FeO, Na₂O, and CaO. FeO is derived from the decomposition of Fe₂O₃;
 584 Na₂O and CaO are derived from the chlorination reaction of NaCl-CaCl₂ with Fe₂O₃. Their
 585 production should be small. However, the theoretical decomposition potentials of CaO and Na₂O
 586 calculated from the thermodynamic software Factsage^[48] are about -2.9 V and -2.6 V, respectively,
 587 which are far more negative than -1.55 V. The theoretical decomposition potential of FeO is -1.32
 588 V, so the reduction at about -1.25 to -1.55 V is considered to be the reduction of Fe²⁺ to Fe.
 589 Unfortunately, the reduction reaction at about -1.25 to -1.55 V was not investigated in this work.

590 Further analysis of the reversal CPs (see Figure 4(a)) is to determine the reduction transition
 591 time and plot the $I - I\tau^{1/2}$ relation. The plot compares closely to a horizontal linear relation, as
 592 shown in Figure 4(b). Likewise, based on the Sand Equation (Eq. [5]), the diffusion coefficient of
 593 Fe³⁺ ions is derived to be (7.5±0.7)×10⁻⁵ cm² s⁻¹, which is utterly consistent with that from Figure
 594 9(b). It is noteworthy that the CP at -14 mA is tested twice, and complete superposition of two

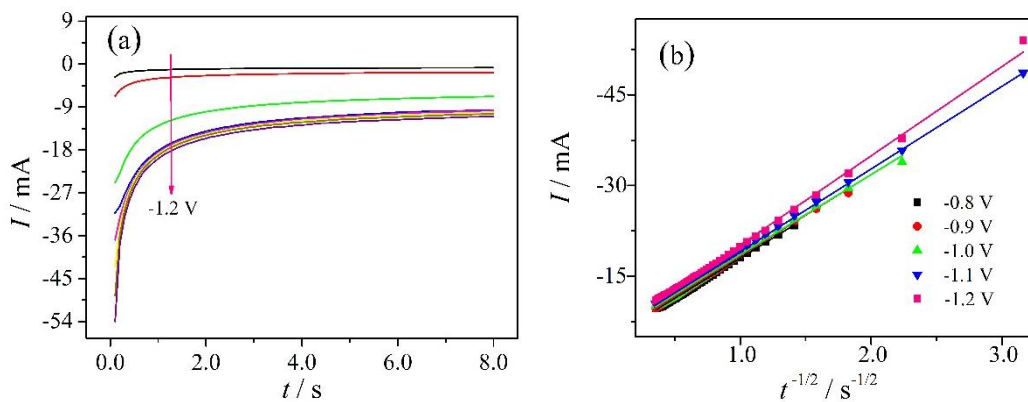
595 corresponding curves is observed, as shown in Figure 9(a). Almost exactly the same values of the
 596 diffusion coefficient obtained from the CPs (Figure 9(b)) and the reversal CPs (Figure 4(b)) as
 597 well as the results of repeated test of the CP at -14 mA shown in Figure 9(a) suggest that the
 598 experimental cell system is stable in nature, with excellent reproducibility and reliable result of
 599 electrochemical test.

600

601 D. Chronoamperometry

602 In order to observe nucleation behavior and confirm whether the electrode process is
 603 controlled by diffusion, the CA tests were performed at different applied potentials. Figure 10(a)
 604 displays the CAs recorded in the melt with 0.5 wt pct Fe₂O₃ at 1273 K, from which no nucleating
 605 behavior is observed,^[7,9,78] possible due to alloying of reduction product Fe and the electrode. It
 606 can be inferred that no nucleation controlled the kinetics of the electrodeposition mechanism of
 607 iron in the eutectic CaCl₂-NaCl melt at 1273 K. When the step potential is applied on the WE,
 608 three cases can be observed with corresponding limited current I_{lim} . Firstly, when the step potential
 609 is low (-0.5, -0.6 V), the limited current I_{lim} is approximately equal to zero, and this is because the
 610 step potential is not high enough to trigger the reduction reaction of Fe³⁺, together with electronic
 611 conduction current and current produced by reduction of foreign ions. Secondly, when the step
 612 potential reaches -0.7 V, the current quickly falls in initial period, indicating deposition reaction of
 613 Fe³⁺; this step potential is utterly consistent with the reduction potential of Fe³⁺ observed by CV,
 614 SWV, and CP described above, with notable increase of the limited current, but not reaching the
 615 maximum stable value. Thirdly, with negative increase in the step potential, the current quickly
 616 falls in the initial period. This is because of the deposition reaction of Fe³⁺ on the Pt WE leading to
 617 rapid decrease of Fe³⁺ concentration near the electrode, to the extent it is too late for Fe³⁺ in the
 618 melt to diffuse to the surface of WE, resulting in sharp attenuation of current; then, the current
 619 slowly decreases and remains stable at I_{lim} . At this time, the diffusion of Fe³⁺ ions to the surface of
 620 the WE reaches the balance with the deposition.

621



622

623 Fig. 10—CAs recorded in the melt with 0.5 wt pct Fe₂O₃ at 1273 K at different step potentials of
 624 -0.5, -0.6, -0.7, -0.8, -0.9, -1.0, -1.1, -1.2 V (a) and the correlation between the cathodic current I
 625 and the $t^{-1/2}$ value at different step potentials of -0.8, -0.9, -1.0, -1.1, -1.2 V (b). RE: O²⁻ |YSZ| Pt |

626 O₂ (air).

627

628 It can be inferred that the reduction reaction at the applied potentials from -1.0 to -1.2 V in
629 Figure 10(a) is not the same as that at the second plateau potentials from -1.25 to -1.55 V in Figure
630 9(a). The explanation is as follows:

631 Firstly, from Figure 10(a), the negative shift in potential from -0.8 to -1.2 V does not affect
632 the value of the current. Thus, the stable currents at these potentials (where the diffusion reached
633 the limit rate) have little difference, but are larger than that at -0.7 V (where the diffusion did not
634 reach the limit rate). The reduction reaction taking place at potentials from -0.7 to -1.2 V should be
635 the same. Under the experimental conditions, it is obviously unreasonable that the reaction at -0.7
636 V was considered as the reduction of Fe³⁺ to Fe and that at the adjacent potentials from -0.8 to -1.2
637 V as another reduction reaction.

638 Secondly, in Figure 9(a), when the applied current is in the range of -11 to -14 mA, the
639 second potential plateau on the CPs appears in the range from -1.25 to -1.55 V in addition to the
640 first potential plateau at about -0.8 V. It can be seen that the potential plateau resulted from an
641 applied current is not the only one in the CPs. That is, the reactions at different potential plateaus
642 cannot be determined directly by only the applied current in the CPs. Similarly, the reactions
643 cannot be determined directly by only the stable currents in the CAs and should be judged in
644 conjunction with the applied potential. It is noted that the second plateau potential in the CPs is
645 more negative than the applied potentials from -0.8 to -1.2 V in the CAs. Therefore, the reaction at
646 applied potentials from -0.8 to -1.2 V in the CAs should be different from that at the plateau
647 potentials from -1.25 to -1.55 V corresponding to the applied currents from -11 to -14 mA in the
648 CPs. Moreover, in this work, there is no *IR* compensation in the CAs, so that the corresponding
649 reaction at the applied potentials from -0.8 to -1.2 V actually takes place at a less negative
650 potential, which approaches the reaction potential revealed by the CVs, the SWVs, and the CPs,
651 and widens the gap from the second plateau potential.

652 For the part of data involving Fe³⁺ reduction and the limited current reaching maximum
653 stable value (*i.e.*, above-mentioned case 3) in Figure 10(a), draw corresponding $I - t^{-1/2}$ curve, as
654 shown in Figure 10(b). It is seen that within the range of 0.5~8 seconds, $I - t^{-1/2}$ is in good linear
655 relation, suggesting the reduction of Fe³⁺ to Fe is a diffusion controlled process within the range.
656 The diffusion controlled current conforms to the Cottrell Equation (Eq. [6]):^[1,79]

$$657 \quad I = -nFAC_0D^{1/2}\pi^{-1/2}t^{-1/2} \quad [6]$$

658 where t is the electrolysis time, seconds. Eq. [6] is analogous to Eq. [5]. It is applicable to the case
659 where the mass transport is controlled by semi-infinite linear diffusion at a constant applied
660 potential.

661 Based on Eq. [6] and fitting $I - t^{-1/2}$ straight line part in Figure 10(b), the diffusion coefficients
662 at variable step potentials are calculated from the slopes of fitting the straight line. Final diffusion

663 coefficient value is obtained as $(4.8\pm 0.2)\times 10^{-5}$ cm² s⁻¹ by horizontal fitting the diffusion
664 coefficients of Fe³⁺ at each step potential.

665

666 *E. Supplementary Discussion*

667 Table II collects the diffusion coefficients of Fe³⁺ derived from multiple testing techniques
668 such as the CV, the SWV, the CP, and the CA in this work. These values are found to be
669 consistent in allowable error, despite of different measuring principles and methods, suggesting it
670 is rational to have the experimental data processed with related equations described above.
671 Although these equations come from the classical electrochemistry where they are mostly
672 established in aqueous solutions, it is known that molten salts like aqueous solutions are also
673 electrolyte solutions, so that the equations can be used to analyze electrochemical data obtained in
674 molten salts when the application conditions on these equations are satisfied. Also, the diffusion
675 coefficients of Fe³⁺ reported in related literature are compared in Table II. Taking into account
676 different experimental conditions and test methods, it is believed that the results described herein
677 match well with recorded values of the literature, suggesting our research methods are feasible to
678 build the integrated electrochemical cell with zirconia-based solid electrolyte tube.

679 It should be noted that the reversibility of an electrode reaction depends on if the ratio of the
680 product and reactant activities obeys the Nernst equation at the electrode/electrolyte interface, but
681 not by the form of the reaction product. When the reaction product is in a solid phase, its activity
682 at the electrode/electrolyte interface would be either constant (pure metal or intermetallic
683 compound) or variable (alloy). Thus, the reversibility can still be checked by the CV and the
684 SWV.^[80] In this work, the obtained CVs have three typical characteristics of a reversible reaction,
685 although reduction product Fe forms an alloy with the Pt electrode. These CV features indicate
686 that alloying has no significant effect on the reversibility of reduction reaction. The calculated
687 results from the CV, the SWV, the CP, the reversal CPs, and the CA, including the number of
688 exchanged electrons and the diffusion coefficient of ferric ions, are in agreement with each other,
689 indicating that the conclusion on the reversibility of the electrode process is reasonable under the
690 present conditions.

691 In this work, Pt was chosen as the WE mainly due to its better chemical and electrochemical
692 stability against oxidation in molten salt although it formed the alloy with reduction product Fe. It
693 should be pointed out that the experimental results with good stability and reproducibility are
694 obtained when the Pt electrode is used as the WE. The authors also acknowledge that it still
695 remains a great challenge to find the suitable inert electrode for electrolytic reduction of iron oxide
696 to iron in molten electrolytes. It is known that graphite reacts with Fe₂O₃ in the melt at the
697 working temperature and hence cannot be used as the WE in this work. On the other hand, the
698 effort to use other WE materials, including low carbon steel, molybdenum, and tungsten, is still
699 ongoing and we hope to publish the findings separately in the near future.

700 In addition, the key part of the integrated cell is the YSZ tube. It is understandable that the

701 stability of the YSZ in the molten salt is a basic necessity to obtain reliable experimental results.
702 In this work, the experimental time in one measurement during one thermal cycle usually lasted
703 for about six hours at high temperatures. In the experiment, erosion of the YSZ tube was never
704 visible, and the reproducibility and consistency of the experimental results not only showed that
705 there was no erosion, but also showed that the RE was stable. Unfortunately, long time electrolysis
706 tests were not performed in this work. It should also be possible to maintain the stability of the RE
707 within a desired accuracy for a long time in practice.

708 It should also be noted that the working temperature of 1273 K studied in this work seems a
709 little too high when heat loss and salt evaporation are significant. However, higher temperatures
710 will also bring about both thermodynamic (lower Gibbs free energy) and kinetic (faster reaction)
711 benefits to the electrode reactions, in addition to the higher conductivity of the YSZ membrane. It
712 is common knowledge that for the same number of joules, electric energy and reaction energy are
713 both of higher prices than that of heat. Thus, from the viewpoint of energy economy, a higher
714 working temperature is not necessarily more expensive for an electrolytic process. The salt loss
715 *via* vaporization at higher temperatures could, however, be problematic, but the liquid mixture of
716 CaCl₂ and NaCl is expected to deviate from the ideal mixture, and hence evaporate less than the
717 pure component salt alone at the same temperature. We also anticipate a lower vapor pressure of
718 the mixture of molten salts when the concentration of dissolved metal oxides approaches to
719 saturation. In addition, the operating temperature is considered not to be the focus in the work
720 because it is limited by some factors such as the resistance of YSZ tube. For the case in this work,
721 if the wall of YSZ tube used became thinner, or Y₂O₃ and Yb₂O₃ co-doped zirconia tube was
722 employed, [81,82] so as to decrease the resistance of zirconia membrane, the operating temperature
723 of the integrated cell would be lower than 1273 K, and the evaporation of molten salt would also
724 reduce.

725

726 IV. CONCLUSIONS

727 A unique integrated three-electrode cell with the “O²⁻ |YSZ | Pt | O₂ (air)” RE was constructed
728 using yttria-stabilized zirconia (YSZ) solid electrolyte tube with a closed end. Electrochemical
729 behavior of ferric ions was systematically investigated in the molten CaCl₂-NaCl eutectic mixture
730 containing 0.5 wt pct Fe₂O₃ at 1273 K. The test results of various electrochemical techniques, such
731 as CV, LSV, SWV, CP, reversal CP, CA, suggest that the reduction of Fe³⁺ to Fe on the Pt WE
732 could be a single one-step and diffusion-controlled reaction that was also possibly reversible. The
733 peak potential of the reduction of Fe³⁺ to Fe on the CV was observed at about -0.73 V, and the
734 reduction product, Fe, was found to alloy with the Pt electrode. The diffusion coefficient of ferric
735 ions was derived in satisfactory consistency from the CV, SWV, CP, reversal CP, and the CA
736 analyses, and also matched reasonably well with those values in related literature. It was found
737 that there was another reduction reaction with potentials more negative than -1.2 V in CPs. It was
738 considered that the reduction reaction was most likely due to the reduction of Fe²⁺ ions from FeO.

739 However, it still needs further investigation and confirmation. The transport of O²⁻ ions in the YSZ
740 membrane seemed to have no or little effect on the behavior of electroactive species on the Pt WE
741 in the three-electrode cell at a sufficiently high temperature. Overall, this work has demonstrated
742 the feasibility of electrochemical investigation of ferric ions in molten salts with the aid of the
743 integrated cell with the “O²⁻| YSZ | Pt | O₂ (air)” RE. We also hope that this work could provide a
744 universal potential reference for the study of other electroactive oxides dissolved in molten salts. It
745 should be noted that the integrated cell as reported in this work is not studied for direct industrial
746 adaption, but the working principle, *i.e.*, using the YSZ membrane for incorporation of RE and
747 also separation of the anode and cathode should be applicable in a future continuous electrolytic
748 steelmaking process, such as the MOE method proposed by Sadoway and co-workers.

749

750 ACKNOWLEDGEMENTS

751 The authors acknowledge funding provided by the National Natural Science Foundation of
752 China (Grant No. 51174148) and the Key Program of Joint Funds of the National Natural Science
753 Foundation of China and the Government of Liaoning Province (Grant No. U1508214).

754

755 REFERENCES

- 756 [1] Y. Castrillejo, A. M. Martinez, M. Vega and P. S. Batanero: *J. Appl. Electrochem.*, 1996, vol.
757 26, pp. 1279-85.
- 758 [2] A. Lugovskoy, M. Zinigrad, D. Aurbach and Z. Unger: *Electrochim. Acta*, 2009, vol. 54, pp.
759 1904-08.
- 760 [3] G. M. Haarberga and M. Keppertb: *Ecs. Trans.*, 2009, vol. 16, pp. 309-15.
- 761 [4] S. Licht and H. Wu: *J. Phys. Chem. C.*, 2011, vol. 115, pp. 25138-47.
- 762 [5] H. Yin, D. Tang, H. Zhu, Y. Zhang and D. Wang: *Electrochem. Commun.*, 2011, vol. 13, pp.
763 1521-24.
- 764 [6] C. Donath, E. Neacsu and N. Ene: *Rev. Roum. Chim.*, 2011, vol. 56, pp. 763-69.
- 765 [7] G. M. Haarberg, E. Kvalheim, S. Rolseth, T. Murakami, S. Pietrzyk and S. Wang: *Ecs.*
766 *Trans.*, 2007, vol. 3, pp. 341-45.
- 767 [8] L. Li, X. Liu and S. Wang: in *Energy Technology 2014: Carbon Dioxide Management and*
768 *Other Technologies*, Eds.: C Wang, J Bakker, C. K. Belt, A. Jha, N. R. Neelameggham, S.
769 Pati, L. H. Prentice, G. Tranell and K. S. Brinkman, John Wiley & Sons, Inc. 2014, pp.
770 135-40.
- 771 [9] S. L. Wang, G. M. Haarberg and E. Kvalheim: *J. Iron Steel. Res. Int.*, 2008, vol. 15, pp.
772 48-51.
- 773 [10] M. A. Quader, S. Ahmed, S. Z. Dawal and Y. Nukman: *Renew. Sust. Energ. Rev.*, 2016, vol.
774 55, pp. 537-49.

- 775 [11] S. Jahanshahi, J. G. Mathieson and H. Reimink: *J. Sustain. Metall.*, 2016, vol. 2, pp. 185-90.
- 776 [12] A. Allanore, L. Yin and D. R. Sadoway: *Nature*, 2013, vol. 497, pp. 353-56.
- 777 [13] D. H. Wang, A. J. Gmitter and D. R. Sadoway: *J. Electrochem. Soc.*, 2011, vol. 158, pp.
- 778 E51-54.
- 779 [14] A. H. C. Sirk, D. R. Sadoway and L. Sibille: *Ecs. Trans.*, 2010, vol. 28, pp. 367-73.
- 780 [15] A. Allanore: *Electrochim. Acta*, 2013, vol. 110, pp. 587-592.
- 781 [16] A. Allanore: *J. Electrochem. Soc.*, 2015, vol. 162, pp. E13-E22.
- 782 [17] G. Z. Chen, D. J. Fray and T. W. Farthing: *Nature*, 2000, vol. 407, pp. 361-64.
- 783 [18] H. Gao, X. Jin, S. Zou, F. Ling, J. Peng, Z. Wang and G. Z. Chen: *Electrochim. Acta*, 2013,
- 784 vol. 107, pp. 261-68.
- 785 [19] G. Li, D. Wang and Z. Chen: *J. Mater. Sci. Technol.*, 2009, vol. 25, pp. 767-71.
- 786 [20] D. Tang, H. Yin, W. Xiao, H. Zhu, X. Mao and D. Wang: *J. Electroanal. Chem.*, 2013, vol.
- 787 689, pp. 109-16.
- 788 [21] A. Cox and D. J. Fray: *J. Appl. Electrochem.*, 2008, vol. 38, pp. 1401-07.
- 789 [22] Y. Berghoute, A. Salmi and F. Lantelme: *J. Electroanal. Chem.*, 1994, vol. 365, pp. 171-77.
- 790 [23] K. K. Kasem and S. Jones: *Platinum Metals Rev.*, 2008, vol. 52, pp. 100-06.
- 791 [24] D. J. Fray: *Metall. Mat. Trans. B*, 2003, vol. 34, pp. 589-94.
- 792 [25] M.J.U.T. Van Wijngaarden, R. J. Dippenaar and P. M. Van Den Heever: *J. S. Afr. Inst. Min.*
- 793 *Metall.*, 1987, vol. 87, pp. 269-78.
- 794 [26] Y. M. Gao, J. X. Song, Y. Q. Zhang and X. M. Guo: *Acta Metall. Sin.*, 2010, vol. 46, pp.
- 795 277-81.
- 796 [27] R. Ganesan, T. Gnanasekaran and R. S. Srinivasa: *J. Nucl. Mater.*, 2006, vol. 349, pp. 133-49.
- 797 [28] T. Ogura, R. Fujiwara, R. Mochizuki, Y. Kawamoto, T. Oishi and M. Iwase: *Metall. Trans. B*,
- 798 1992, vol. 23B, pp. 459-66.
- 799 [29] E.T. Turkdogan: *Ironmaking Steelmaking*, 2000, vol. 27, pp. 32-36.
- 800 [30] P. Soral, U. Pal, H. R. Larson and B. Schroeder: *Metall. Mat. Trans. B*, 1999, vol. 30B, pp.
- 801 307-21.
- 802 [31] W. Kim, D. J. Min, Y. S. Lee and J. H. Park: *ISIJ Int.*, 2009, vol. 49, pp. 1882-88.
- 803 [32] X. Guan, S. Su, U. B. Pal and A. C. Powell: *Metall. Mat. Trans. B*, 2014, vol. 45B, pp.
- 804 2138-44.
- 805 [33] A. Krishnan, X.G. Lu and U.B. Pal: *Metall. Mat. Trans. B*, 2005, vol. 36B, pp. 463-73.
- 806 [34] E. S. Gratz, X. Guan, J. D. Milshtein, U. B. Pal and A. C. Powell, *Metall. Mat. Trans. B*,
- 807 2014, 45B, pp. 1325-36.
- 808 [35] Y. M Gao, C. Duan, Y. B. Yang, D. Ruan, C. H. Yang and C. Hong: *ISIJ Int.*, 2015, vol. 55,
- 809 pp. 2273-82.
- 810 [36] Y. M. Gao, B. Wang, S. B. Wang and S. Peng: *Journal of Mining and Metallurgy, Section B:*
- 811 *Metallurgy*, 2013, vol. 49, pp. 49-55.
- 812 [37] C. Mallika, O. M. Sreedharan and R. Subasri: *J. Eur. Ceram. Soc.*, 2000, vol. 20, pp.

813 2297-2313.

814 [38] S. C. Britten and U. B. Pal: *Metall. Mater. Trans. B*, 2000, vol. 31B, pp. 733-53.

815 [39] C. Z. Wang: *Solid Electrolyte and Chemical Sensors*, Metallurgical Industry Press, Beijing,

816 2000.

817 [40] N. Otsuka: *ECS Transactions*, 2012, vol. 41, pp. 13-19.

818 [41] S. H. Cho, D. Y. Kim, S. Kwon, B. H. Yoon and J. H. Lee: *J. Nucl. Sci. Technol.*, 2018, vol.

819 55, pp.97-103.

820 [42] S.H. Cho, S.W. Kim, D.Y. Kim, J.H. Lee and J.M. Hur: *J. Nucl. Mater.*, 2017, vol. 490,

821 pp.85-93.

822 [43] Y. Gao, C. Yang, C. Zhang, Q. Qin and G. Z. Chen: *Phys. Chem. Chem. Phys.*, 2017, vol. 19,

823 pp. 15876-90.

824 [44] Y. Gao, C. Hong and C. Yang: *J. Electrochem. Soc.*, 2015, vol. 162, pp. E362-69.

825 [45] K. Igarashi, H. Ohtani and J. Mochinaga: *Z. Für Naturforsch. A*, 1987, vol. 42A, pp.

826 1421-24.

827 [46] X. Y. Chen: *Solubility of oxides in molten salts and the preparation of carbide-derived*

828 *carbon by fused salt electrolysis process* (Master's Thesis), Northeastern University,

829 Shenyang, 2012.

830 [47] G. M. Haarberg, E. Kvalheim and S. Rolseth: Electrochemical behaviour of dissolved iron

831 species in molten salts, in *Molten Salts XIV - Proceedings of the International Symposium*,

832 R.A. Mantz et al, Editors, PV 2004-24, The Electrochemical Society Proceedings Series,

833 Pennington, NJ, 2004, p. 890.

834 [48] Factsage 7.1 (Centre for Research in Computational Thermochemistry (CRCT) and

835 GTT-Technologies, 2017), <http://www.factsage.com/>. Accessed 2 August 2017.

836 [49] J. Yu, W. Yi, B. Chen and H. Chen: *Binary Alloy Phase Diagrams*, Shanghai Scientific and

837 Technical Publishers, Shanghai, 1987, pp. 371.

838 [50] H. E. Ghallali, H. Groult, A. Barhoun, K. Draoui and D. Krulic: *Electrochim. Acta*, 2009, vol.

839 54, pp. 3152-60.

840 [51] A. J. Bard and L. R. Faulkner: *Electrochemical Methods Fundamentals and Applications*,

841 2nd Ed., John Wiley & Sons, Inc, New York, 2001, pp. 226-61.

842 [52] A. J. Bard and L.R. Faulkner: *Electrochemical Methods Fundamentals and Applications*, 2nd

843 Ed., John Wiley & Sons, Inc, New York, 2001, pp. 669-76.

844 [53] H. Tang and B. Pesic: *Electrochim. Acta*, 2014, vol. 119, pp. 120-30.

845 [54] M. Gibilaro, L. Massot, P. Chamelot, L. Cassayre and P. Taxil: *Electrochim. Acta*, 2013, vol.

846 95, pp. 185-91.

847 [55] M. Jayakumar, K. A. Venkatesan and T. G. Srinivasan: *Electrochim. Acta*. 2008, vol. 53, pp.

848 2794-2801.

849 [56] T. Sakurada, H. Maekawa and T. Yokokawa: *Mater. Trans.*, 2007, vol. 39, pp. 740-46.

850 [57] Q. R. Shi, S. Z. Duan and S. M. Wu: *J. Univ. Sci. Technol. B.*, 1994, vol. 16, pp. 599-603.

851 [58] W. Huang, L. Tian, C. She, F. Jiang, H. Zheng, W. Li, G. Wu, D. Long and Q. Li:
852 *Electrochim. Acta*, 2014, vol. 147, pp. 114-20.

853 [59] Z. Chen, Y. J. Li and S. J. Li: *J. Alloys Compd.*, 2011, vol. 509, pp. 5958-61.

854 [60] C. Nourry, P. Souček, L. Massot, R. Malmbeck, P. Chamelot and J.-P. Glatz: *J. Nucl. Mater.*,
855 2012, vol. 430, pp. 58-63.

856 [61] F. H. Hu: *Molten Salt Physical Chemistry*, China Industry Press, Beijing, 1963, pp.73-96.

857 [62] D. Shuzhen, P. Dudley and D. Inman: *J. Electroanal. Chem. Interf. Electrochem.*, 1982, vol.
858 142, pp. 215-28.

859 [63] B. Khalaghia, E. Kvalheima, M. Tokushige, L. Teng, S. Seetharamanc and G. M. Haarbergd:
860 *ECS Trans.*, 2014, vol. 64, pp. 301-10.

861 [64] Z. Guangwen, L. Yupin and Z. Yuankai: *Journal of Beijing iron and steel institute*, 1983, (2):
862 68-78.

863 [65] L. Massot, P. Chamelot and F. Bouyer: *Electrochim. Acta*, 2002, vol. 47, pp. 1949-57.

864 [66] S. Frangini and S. Scaccia: *J. Electrochem. Soc.*, 2005, vol.152, pp. A2155-58.

865 [67] V. A. Volkovich, T. R. Griffiths, D. J. Fray and R. C. Thied: *J. Nucl. Mater.*, 2000, vol. 282,
866 pp. 152-58.

867 [68] M. Hayyan, M. A. Hashim and I. M. AlNashef: *Chem. Rev.*, 2016, vol. 116, pp. 3029-85.

868 [69] P. G. Zambonin: *J. Phys. Chem.*, 1974, vol. 78, pp. 1294-98.

869 [70] M. Chandra, S. Vandarkuzhali, S. Ghosh, N. Gogoi, P. Venkatesh, G. Seenivasan, B. P.
870 Reddy and K. Nagarajan: *Electrochim. Acta*, 2011, vol. 58, pp. 150-56.

871 [71] C. Hamel, P. Chamelot and P. Taxil: *Electrochim. Acta*, 2004, vol. 49, pp. 4467-76.

872 [72] A. Wiedenroth and C. Rüssel: *J. Non-Cryst. Solids*, 2004, vol. 347, pp. 180-86.

873 [73] A. Wiedenroth and C. Rüssel: *J. Non-Cryst. Solids*, 2001, vol. 290, pp. 41-48.

874 [74] E. Freude: *Voltammetrische Untersuchung des Redoxverhaltens polyvalenter Ionen in*
875 *Glasschmelzen*, insbesondere von Technetium, Thesis Erlangen, 1989.

876 [75] C. Rüssel and E. Freude: *Glastech. Ber.*, 1990, vol. 63, pp. 149-53.

877 [76] O. Claussen and C. Rüssel: *Glastech. Ber. Glass Sci. Technol.*, 1996, vol. 69, pp. 95-100.

878 [77] A.W.M. Wondergem·de Best: *Redox behaviour and fining of molten glass* (Doctoral Thesis),
879 Technische Universiteit Eindhoven, 1994, pp. 126

880 [78] K. Serrano and P. Taxil: *J. Appl. Electrochem.*, 1999, vol. 29, pp. 505-10.

881 [79] A. J. Bard and L. R. Faulkner: *Electrochemical Methods Fundamentals and Applications*,
882 2nd Ed., John Wiley & Sons, Inc, New York, 2001, pp. 161-65.

883 [80] J. De Strycker, P. Westbroek and E. Temmerman: *J. Electroanal. Chem.*, 2004, vol. 565,
884 pp.149-58.

885 [81] Y. M. Kan, S. L. Li, P. L. Wang, G. J. Zhang, O. V. de Biest and J. Vleugels: *Solid State*
886 *Ionics*, 2008, vol. 179, pp. 1531-1534.

887 [82] Z. G. Lv, P. Yao, R. S. Guo and F.Y. Dai: *Mat. Sci. Eng. A*, 2007, vol. 458, pp. 355-360.

888

889

890 **Tables:****Table I. Transition Time Data from Fig. 4(a).**

I (mA)	τ_{red} (s)	τ_{ox} (s)	$\tau_{\text{red}}/\tau_{\text{ox}}$
± 10	—*	1.63	—
± 11	7.40	1.41	5.2
± 12	5.13	1.17	4.4
± 13	4.00	1.10	3.6
± 14	3.05	1.04	2.9

I applied current, τ_{red} Reduction transition time, τ_{ox} oxidation transition time.

* The exact value cannot be obtained.

891

892

Table II. Collections for Diffusion Coefficients of Ferric Ions in Similar Molten Halide Salts.

Salt composition (Weight Percent)	Fe ₂ O ₃ (Weight Percent)	WE/RE	MT	$D \times 10^5$ (cm ² s ⁻¹)	T (K)	Refs.
65CaCl ₂ -35NaCl	0.5	Pt/YSZ Pt O ₂ (air)	CV	4.9±0.5 [†]	1273	This work
				1.8±0.1 [‡]		
			SWV	6.7±0.4 [†]		
				2.4±0.1 [‡]		
				7.5±0.6		
			CP	7.5±0.7		
				Reversal CP		
			CA	4.8±0.2		
CaCl ₂ -NaCl*	0.28	Mo/Ag	CV	9.4±0.7	1123	6
85CaCl ₂ -15CaF ₂	0.6	Mo/Pt	CV	3**	1100	7
79CaCl ₂ -9.7CaF ₂ -11.3KF	0.4	Mo/Fe	CV	5.3	1100	8
89.1CaCl ₂ -10.9KF	0.4	Mo/Fe	CV	9.7	1100	8
90CaCl ₂ -10KF	0.6	Mo/Pt	CV	9.7	1100	9

WE/RE, working electrode/reference electrode; MT, measurement technique; CV, cyclic voltammetry; SWV, square wave voltammetry; CP, chronopotentiometry; CA, chronoamperometry.

* The proportion of CaCl₂ and NaCl is not found in the paper.

** The calculation process is unknown from the paper.

[†]Passing through the origin.

[‡]Not passing through the origin.

893

894

895

896 **Figure Captions:**

897

898 Fig. 1—Schematic illustration of the YSZ-based integrated three-electrode cell for
899 electrochemical analyses in molten salt at high temperatures (1273 K in this work).

900

901 Fig. 2—A typical OCP-time plot recorded in the course of immersing the Pt wire WE into the
902 molten mixture containing 0.5 wt pct Fe₂O₃ and then switching from Ar to air in the furnace tube
903 (a); a typical WE potential-time curve recorded in the polarization experiment (b), and a typical
904 AC impedance Nyquist plot recorded at the OCP (bias potential) (c). RE: O²⁻ | YSZ | Pt | O₂ (air).

905

906 Fig. 3—CVs recorded in molten CaCl₂-NaCl at 1273 K with 0.5 wt pct Fe₂O₃ at ν (potential scan
907 rate) = 0.04, 0.05, 0.06, 0.07, 0.08, 0.10, 0.50, or 1.00 V s⁻¹, and without Fe₂O₃ (blank) at $\nu = 50$
908 mV s⁻¹ (a), and correlations of I_{pc} (reduction peak current) and E_{pc} (reduction peak potential) with
909 $\nu^{1/2}$ (b). RE: O²⁻ | YSZ | Pt | O₂ (air).

910

911 Fig. 4—Reversal CPs on the Pt WE in molten CaCl₂-NaCl with 0.5 wt pct Fe₂O₃ at 1273 K and
912 different currents (± 10 , ± 11 , ± 12 , ± 13 and ± 14 mA) (a) and the correlation of the $I\tau^{1/2}$ (τ
913 transition time) value against the cathodic current I for the reduction plateau (b). RE: O²⁻ | YSZ | Pt
914 | O₂ (air).

915

916 Fig. 5—LSVs recorded at 50 mV s⁻¹ on the Pt wire WE under the static and rotating modes after
917 the potentiostatic electrolysis for 30, 60, 90 seconds in molten CaCl₂-NaCl with 0.5 wt pct Fe₂O₃.
918 Inset: a set of typical current-time curves of potentiostatic electrolysis using the Pt wire WE for 30,
919 60, 90 seconds. Potentiostatic electrolysis potential: -0.76 V; time: 30, 60, 90 s; temperature: 1273
920 K; RE: O²⁻ | YSZ | Pt | O₂ (air).

921

922 Fig. 6—SEM image of the cross section of the Pt wire WE (a), EDS analyses of spots 1 and 2 in
923 the SEM image (b), and the line scanning profiles of Pt (c), Fe (d) and O (e) after potentiostatic
924 electrolysis in molten CaCl₂-NaCl with 0.5 wt pct Fe₂O₃. Potentiostatic electrolysis potential: -
925 0.73 V; time: 30 min; temperature: 1273 K; RE: O²⁻ | YSZ | Pt | O₂ (air).

926

927 Fig. 7—XRD pattern for the Pt foil WE after potentiostatic electrolysis in molten CaCl₂-NaCl
928 with 0.5 wt pct Fe₂O₃. Potentiostatic electrolysis potential: - 0.7 V; time: 30 min; temperature:

929 1273 K; RE: O²⁻ | YSZ | Pt | O₂ (air).

930

931 Fig. 8—SWVs recorded in the molten CaCl₂-NaCl mixture with 0.5 wt pct Fe₂O₃ at different
932 frequencies (30, 40, 50, 60, 70, 80 Hz) and 1273 K (*a*) and the correlations between the peak
933 current (*I_p*), the peak potential (*E_p*), and the square root of the frequency (*f^{1/2}*), respectively (*b*).

934 RE: O²⁻ | YSZ | Pt | O₂ (air).

935

936 Fig. 9—CPs recorded in the melt with 0.5 wt pct Fe₂O₃ at 1273 K at different cathodic currents of
937 -8, -10, -11, -12, -13, -14, -14 mA (*a*) and the correlation between the cathodic current *I* and the
938 *Iτ^{1/2}* (*τ*: transition time) value for the reduction plateau (*b*). RE: O²⁻ | YSZ | Pt | O₂ (air).

939

940 Fig. 10—CAs recorded in the melt with 0.5 wt pct Fe₂O₃ at 1273 K at different step potentials of
941 -0.5, -0.6, -0.7, -0.8, -0.9, -1.0, -1.1, -1.2 V (*a*) and the correlation between the cathodic current *I*
942 and the *t^{-1/2}* value at different step potentials of -0.8, -0.9, -1.0, -1.1, -1.2 V (*b*). RE: O²⁻ | YSZ | Pt |

943 O₂ (air).